Dalton Transactions

ROYAL SOCIETY OF CHEMISTRY

PAPER

View Article Online
View Journal | View Issue

Cite this: *Dalton Trans.*, 2025, **54**, 11743

Mn(III) porphyrins as photosensitizers: structural, photophysical and anticancer studies†

Bidisha Bora,[a] Namisha Das,[a] Jakia Parbin Sultana,[a] Md Kausar Raza *[b] and Tridib K. Goswami *[a]

Herein, we synthesized, characterized and explored the photo-triggered anticancer activity of five Mn(III) porphyrins **Mn1–Mn5**, *viz.* (diaqua)*meso*-(tetraphenylporphyrinato)manganese(III) propionate, [Mn(III)TPP$(H_2O)_2]^+(C_3H_5O_2^-)$ or **Mn1**; (diaqua)*meso*-tetrakis(4-methylphenylporphyrinato)manganese(III) propionate, [Mn(III)TMeP$(H_2O)_2]^+(C_3H_5O_2^-)$ or **Mn2**; (diaqua)*meso*-tetrakis(4-methoxyphenylporphyrinato)manganese (III) propionate, [Mn(III)TMP$(H_2O)_2]^+(C_3H_5O_2^-)$ or **Mn3**; (diaqua)*meso*-tetrakis(4-fluorophenylporphyrinato) manganese(III) propionate, [Mn(III)FTPP$(H_2O)_2]^+(C_3H_5O_2^-)$ or **Mn4** and (diaqua)*meso*-tetrakis(4-chlorophenylporphyrinato)manganese(III) propionate, [Mn(III)ClTPP$(H_2O)_2]^+(C_3H_5O_2^-)$ or **Mn5**, which remain virtually unexplored as photodynamic therapy (PDT) agents like other paramagnetic metalloporphyrins. These Mn (III) porphyrins, bearing different *para*-substituents on their *meso*-phenyl rings and two water molecules as axial ligands, were characterized using spectroscopic techniques and structurally through single-crystal X-ray diffraction, revealing an octahedral MnN_4O_2 geometry. Binding studies demonstrated a strong affinity of the metalloporphyrins for human serum albumin (HSA), indicating their potential for biological applications. The visible light-assisted generation of reactive oxygen species (ROS) by these Mn(III) porphyrins was confirmed *via* 1,3-diphenylisobenzofuran (DPBF) titration, identifying singlet oxygen ($^1O_2$) as one of the primary ROS. Photoredox activity under visible light, displayed by the Mn(III) porphyrins in the presence of ascorbic acid involving +3 and +2 oxidation states of manganese, further underscores the photochemotherapeutic potential of **Mn1–Mn5**. The ROS generation ability was further validated intracellularly in HeLa cells using **Mn4** with the help of 2′,7′-dichlorofluorescein diacetate (DCFDA) assay under visible light irradiation (λ = 400–700 nm). Furthermore, among the five Mn(III) porphyrin complexes (**Mn1–Mn5**) evaluated for photo-triggered anticancer activity using MTT assays, **Mn4** exhibited superior photocytotoxicity, with a half-maximal inhibitory concentration (IC_{50}) of 4.93 ± 0.7 μM against HeLa cancer cells under visible light irradiation and negligible dark toxicity (IC_{50} > 50 μM). These results suggest that both type-I and type-II ROS generation pathways contribute to the observed photocytotoxicity. This study highlights the potential of paramagnetic metalloporphyrins, particularly Mn(III) porphyrins, in anticancer application by demonstrating their effectiveness as photosensitizers for photodynamic cancer therapy.

Received 11th December 2024,
Accepted 4th July 2025

DOI: 10.1039/d4dt03432e

rsc.li/dalton

Introduction

Porphyrins belong to the family of tetrapyrrolic macrocycles that have gained massive research interest due to their many biological relevance and potential applications in diverse fields such as catalysis, sensing, and medicinal chemistry. Their unique optical, electronic, redox and catalytic properties make them ligands par excellence in both biology and chemistry.[1–4] The use of porphyrins as photosensitizers (PSs) in photodynamic therapy (PDT) has grown considerably over the past few decades as a promising approach to combat cancer. PDT is a recently developed technique that relies on the ability of the PSs to generate cell-damaging reactive oxygen species (ROS) in the presence of light of an appropriate wavelength and molecular oxygen, thereby eliminating malignant cells.[5–7] This therapy offers several advantages over traditional cancer treatments due to its non-invasiveness, spatiotemporal controllability and minimal systemic toxicity.[8–10] Porphyrinic PSs are reported to preferentially accumulate in tumour cells over normal cells and exhibit photocytotoxicity *via* the type-II

[a]*Department of Chemistry, Gauhati University, Guwahati 781014, Assam, India. E-mail: tridibgoswami05@gmail.com*
[b]*Department of Inorganic and Physical Chemistry, Indian Institute of Science, Bangalore 560012, India. E-mail: kausarraza91@gmail.com*

†Electronic supplementary information (ESI) available: Characterization, selected X-ray crystallographic data, HSA binding data (Tables S1–S6, Scheme S1, Fig. S1–S52). CCDC 2408932, 2408982, 2408984 and 2408985 for compounds **Mn1**, **Mn2**, **Mn4** and **Mn5**, respectively. For ESI and crystallographic data in CIF or other electronic format see DOI: https://doi.org/10.1039/d4dt03432e

PDT pathway, *i.e.* through the production of singlet oxygen ($^1O_2$).[8,9,11–13] However, some literature reports suggest that paramagnetic metalloporphyrins are not considered good photosensitizers as they negatively affect the $^1O_2$ generation process.[14,15] Nonetheless, in 2014, Antoni *et al.* reported the photocytotoxicity of a paramagnetic Cu(II) porphyrin in A2780 cancer cell lines, which was attributed to its ability to generate cytotoxic hydroxyl radicals (˙OH) upon exposure to red light.[16] This study prompted us to explore the photocytotoxicity of other paramagnetic metalloporphyrins and their mechanism of action.

Manganese plays an enormous roles in various biological activities, such as crucial roles in different metabolic functions, including cofactor for different type of enzymes, which calls for it use in pharmaceuticals.[17] Mn-porphyrins bearing high positive charges were initially developed as SOD mimics and redox-active antioxidants.[18] Their anticancer activity is thought to result from redox-induced cytotoxicity, which can affect the redox balance of cancer cells.[18–20] However, there are only a few reports on the photoinduced anticancer activity of Mn-porphyrins.[21–23] In 2003, Banfi *et al.* reported that positively charged Mn(III) porphyrins could oxidatively damage Plasmid Bluescript DNA in the presence of either an artificial oxygen donor or light,[21] demonstrating the potential of Mn(III) porphyrins in PDT. In 2017, Lei Shi and co-workers demonstrated considerable photocytotoxicity of an anionic Mn(III) porphyrin in HepG2 cells.[22] More recently, Nemeth and colleagues reported the PDT activity of a cationic Mn(III) pyridyl porphyrin in HeLa cells, and their EPR studies indicated that $^1O_2$ was the primary cytotoxic species.[23] In another study, Kim *et al.* showed that Mn(III) porphyrins undergo photoreduction in the presence of polynucleotides and can oxidize DNA *via* a photo-redox pathway.[24]

With these facts in mind, in this work, we synthesized five Mn(III) porphyrins bearing simple substituents at the *para* position of the *meso*-phenyl rings and two axial aqua ligands, *viz.* (diaqua)*meso*-(tetraphenylporphyrinato)manganese(III) propionate, $[Mn(III)TPP(H_2O)_2]^+(C_3H_5O_2^-)$ or **Mn1**; (diaqua)*meso*-tetrakis(4-methylphenyl porphyrinato)manganese(III) propionate, $[Mn(III)TMeP(H_2O)_2]^+(C_3H_5O_2^-)$ or **Mn2**; (diaqua)*meso*-tetrakis(4-methoxyphenylporphyrinato)manganese(III) propionate, $[Mn(III)TMP(H_2O)_2]^+(C_3H_5O_2^-)$ or **Mn3**; (diaqua)*meso*-tetrakis (4-fluorophenyl porphyrinato)manganese(III) propionate, $[Mn(III)FTPP(H_2O)_2]^+(C_3H_5O_2^-)$ or **Mn4**; and (diaqua)*meso*-tetrakis (4-chlorophenylporphyrinato)manganese(III) propionate, $[Mn(III)ClTPP(H_2O)_2]^+(C_3H_5O_2^-)$ or **Mn5**, in order to examine their photoinduced anticancer activity (Chart 1). The compounds were fully characterized by various spectroscopic and analytical techniques and structurally characterized by single crystal X-ray diffraction. They showed significant binding affinity towards human serum albumin (HSA) protein. UV-visible titration experiments with DPBF confirmed the generation of $^1O_2$ by the compounds. The Mn(III) porphyrins also displayed redox shuttling between Mn(III) and Mn(II) in air in the presence of ascorbic acid and visible light, which is believed to induce additional oxidative stress in cells. Furthermore, 2′,7′-dichlorofluorescein diacetate (DCFDA) assay demonstrated the generation of ROS by the metalloporphyrins in the cellular environment. MTT assays showed significant photocytotoxicity of the Mn(III) porphyrins in HeLa cells under visible light.

Experimental section

Materials and measurements

Chemicals and solvents used in the work were obtained from commercial sources such as SD Fine Chemicals, India; Spectrochem, India; Loba Chemie, India; and Sigma-Aldrich, USA, and were used as received unless otherwise specified. Freshly purified pyrrole, prepared by passing it through a short column of basic alumina, was used for the synthesis of the free bases. Human serum albumin (HSA), 1,3-diphenylisobenzofuran (DPBF), L-ascorbic acid, Dulbecco's modified Eagle's medium (DMEM), MTT (3-(4,5-dimethylthiazol-2-yl)-2,5-diphenyltetrazolium bromide), 2′,7′-dichlorofluorescein diacetate (DCFDA), Dulbecco's phosphate-buffered saline (DPBS) and fetal bovine serum (FBS) were all purchased from Sigma-Aldrich (USA). Tris-(hydroxylmethyl)aminomethane-HCl (Tris-HCl) buffer solution was prepared by using deionised and sonicated double-distilled water.

Elemental CHN analyses were performed using a Thermo Finnigan Flash EA 1112 CHN analyzer. FT-IR spectra were recorded on a Bruker Alpha-II spectrophotometer, with samples prepared as KBr pellets. Electronic absorption and emission spectra were recorded on Shimadzu UV-1800 and Hitachi F-7000 spectrophotometers, respectively. ^1H NMR spectra were recorded at room temperature on Bruker 300 MHz and 400 MHz NMR spectrometers. Room-temperature magnetic susceptibility measurements of the Mn(III) porphyrins were obtained using a Sherwood Scientific instrument (Cambridge, England), with $Hg[Co(NCS)_4]$ as the standard. The experimental susceptibility data were corrected for diamagnetic contributions.[25] Electrochemical measurements were carried out at 25 °C using a CHI660D electrochemical workstation (CH Instruments, Inc., USA) with a conventional three-electrode configuration consisting of a glassy carbon working electrode, platinum wire auxiliary electrode and an Ag/AgCl reference electrode. Tetrabutylammonium perchlorate (TBAP, 0.1 M) in DMF was used as the supporting electrolyte. High-

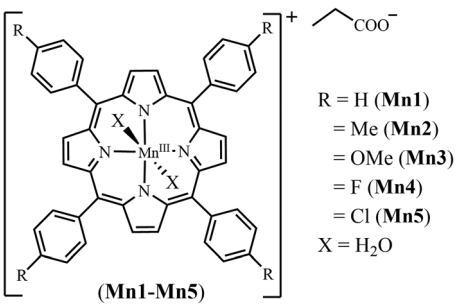

Chart 1 Schematic representations of Mn(III) porphyrins (**Mn1–Mn5**).

resolution electrospray ionization mass spectral measurements were recorded using a Waters Xevo G2-XS QTof mass spectrometer. Photoirradiation for cellular experiments was performed using a Luzchem Photoreactor (model LZC-1, Ontario, Canada) equipped with eight Sylvania white fluorescent tubes (λ = 400–700 nm). A TECAN microplate reader provided the formazan absorbance values in the MTT assay, and the resulting data were analyzed using GraphPad Prism 8 software. A fluorescence-activated cell sorting (FACS) Verse device (BD Biosciences) was used to conduct the flow cytometric analysis. The instrument is equipped with a MoFLo XDP cell sorter and analyzer featuring 10-color detection capability, and three lasers (λ = 488, 365, and 640 nm).

Synthesis

Synthesis of free-base porphyrins (L1–L5). The free-base porphyrins (**L1–L5**) were synthesized following the methodology of Adler *et al.*, in which the precursor aldehydes (40 mmol) were mixed with freshly purified pyrrole (40 mmol) in a 100 mL round-bottom flask containing 50 mL of propionic acid.[26] The solution was refluxed for 30 minutes, then cooled to room temperature and filtered. The filter cake was thoroughly washed with methanol followed by hot water. The crude solid obtained was dried in a vacuum desiccator. The solid was further purified by column chromatography [DCM : petroleum ether (1 : 1)] to obtain the pure ligands as purple crystalline solids [yield: 1.125 g, 19.23% for **L1**; 1.310 g, 19.87% for **L2**; 1.287 g, 19.8% for **L3**; 0.980 g, 14.30% for **L4**; 1.240 g, 16.45% for **L5**] (Scheme S1, ESI†).

Anal. calcd for $C_{44}H_{30}N_4$ (**L1**): C, 85.97; H, 4.92; N, 9.11. Found: C, 85.71; H, 4.87; N, 9.23. Selected IR data (KBr, cm^{-1}): 3314w (N–H), 3052w and 3021w (C–H), 2920w, 1678s, 1592m (C═C), 1553m, 1470s (C═C), 1437s, 1402m, 1347s (C–N), 1219w, 1174s, 1071m, 963vs, 799vs (C–$H_{bending}$), 700vs (vs, very strong; s, strong; m, medium; w, weak; br, broad). UV-Visible in DMSO, [λ_{max}/nm (ε/M^{-1} cm^{-1})]: 416 (S, 1.87×10^5), 513 (Q, 8.42×10^3), 548 (Q, 3.8×10^3), 590 (Q, 2.60×10^3), 647 (Q, 2.56×10^3). ^{1}H NMR (300 MHz, $CDCl_3$): δ ppm, 8.88 (s, 8H, β PyH), 8.25–8.23 (d, J = 6.0 Hz, 8H, Ar *o*-H), 7.79–7.77 (d, J = 6.0 Hz, 12H, Ar *m* & *p* H), −2.76 (s, 2H, NH). ESI-MS in MeOH (*m*/*z*): 615.2551 for $[M + H]^+$ (calcd: 615.2549).

Anal. calcd for $C_{48}H_{38}N_4$ (**L2**): C, 85.94; H, 5.71; N, 8.35. Found: C, 85.73; H, 5.77; N, 8.27. Selected IR data (KBr, cm^{-1}): 3326w (N–H), 3021w (C–H), 2902w, 1699w, 1557m (C═C), 1509m, 1468s (C═C), 1347s (C–N), 1217w, 1180s, 1108w, 1021w, 966vs, 846m, 799vs (C–$H_{bending}$), 733s, 615m. UV-Visible in DMSO, [λ_{max}/nm (ε/M^{-1} cm^{-1})]: 418 (S, 2.8×10^5), 515 (Q, 1.2×10^4), 550 (Q, 6.2×10^3), 593 (Q, 3.5×10^3), 649 (Q, 3.9×10^3). ^{1}H NMR (400 MHz, $CDCl_3$): δ ppm, 8.86 (s, 8H, β PyH), 8.11–8.09 (d, J = 8.0 Hz, 8H, Ar *o*-H), 7.57–7.55 (d, J = 8.0 Hz, 8H, Ar *m*-H), 2.71 (s, 12H, CH_3), −2.78 (s, 2H, NH). ESI-MS in MeOH (*m*/*z*): 671.3177 for $[M + H]^+$ (calcd: 671.3175).

Anal. calcd for $C_{48}H_{38}N_4O_4$ (**L3**): C, 78.45; H, 5.21; N, 7.62. Found: C, 78.21; H, 5.29; N, 7.55. Selected IR data (KBr, cm^{-1}): 3314w (N–H), 2928w (C–H), 2832w (C–H of –OCH_3), 1744m, 1604s (C═C), 1505s, 1464s (C═C), 1347m (C–N), 1289s, 1248vs (C–O–C), 1174vs, 1108w, 1033s, 966s, 803s (C–$H_{bending}$), 737s, 640m. UV-Visible in DMSO, [λ_{max}/nm (ε/M^{-1} cm^{-1})]: 421 (S, 1.77×10^5), 518 (Q, 7.06×10^3), 555 (Q, 5.48×10^3), 595 (Q, 2.40×10^3), 651 (Q, 3.9×10^3). ^{1}H NMR (300 MHz, $CDCl_3$): δ ppm, 8.86 (s, 8H, β PyH), 8.14–8.11 (d, J = 9.0 Hz, 8H, Ar *o*-H), 7.30–7.27 (d, J = 9.0 Hz, 8H, Ar *m*-H), 4.10 (s, 12H, OCH_3), −2.78 (s, 2H, NH). ESI-MS in MeOH (*m*/*z*): 735.2908 for $[M + H]^+$ (calcd: 735.2971).

Anal. calcd for $C_{44}H_{26}N_4F_4$ (**L4**): C, 76.96; H, 3.82; N, 8.16. Found: C, 76.84; H, 3.79; N, 8.22. Selected IR data (KBr, cm^{-1}): 3309m (N–H), 3042w (C–H), 1699w, 1600m (C═C), 1555w, 1503vs, 1470s (C═C), 1400w, 1351m (C–N), 1225vs, 1157vs (Ar–F), 1091w, 968s, 846m, 807vs (C–$H_{bending}$), 729s. UV-Visible in DMSO, [λ_{max}/nm (ε/M^{-1} cm^{-1})]: 414 (S, 4.2×10^4), 511 (Q, 2.7×10^3), 545 (Q, 1.2×10^3), 586 (Q, 7.8×10^2), 645 (Q, 5.7×10^2). ^{1}H NMR (300 MHz, DMSO-d_6 with NaOH): δ ppm, 8.53 (s, 8H, β PyH), 8.14–8.12 (d, J = 6.0 Hz, 8H, Ar *o*-H), 7.57–7.51 (t, J = 9 Hz, 8H, Ar *m*-H). ESI-MS in MeOH (*m*/*z*): 687.4095 for $[M + H]^+$ (calcd: 687.2172).

Anal. calcd for $C_{44}H_{26}Cl_4N_4$ (**L5**): C, 70.23; H, 3.48; N, 7.45. Found: C, 70.11; H, 3.42; N, 7.49. Selected IR data (KBr, cm^{-1}): 3312w (N–H), 2920m (C–H), 2850w, 2310w, 1656w, 1553m (C═C), 1470s (C═C), 1394m, 1344m (C–N), 1174m, 1089vs (Ar–Cl), 1015s, 966s, 844m, 795vs (C–$H_{bending}$), 729s. UV-Visible in DMSO, [λ_{max}/nm (ε/M^{-1} cm^{-1})]: 417 (S, 1.87×10^5), 514 (Q, 8.72×10^3), 549 (Q, 3.67×10^3), 590 (Q, 2.58×10^3), 647 (Q, 2.14×10^3). ^{1}H NMR (300 MHz, $CDCl_3$): δ 8.84 (s, 8H, β PyH), 8.15–8.12 (d, J = 9.0 Hz, 8H, Ar *o*-H), 7.76–7.74 (d J = 6.0 Hz, 8H, Ar *m*-H), −2.88 (s, 2H, NH). ESI-MS in MeOH (*m*/*z*): 753.0969 for $[M + H]^+$ (calcd: 753.0960).

Synthesis of the Mn(III) porphyrins (Mn1–Mn5). The metalloporphyrins (**Mn1–Mn5**) were synthesized using a general procedure, in which the respective free bases (0.25 mmol; 153 mg for **L1**, 167 mg for **L2**, 183 mg for **L3**, 171 mg for **L4**, 188 mg for **L5**) were dissolved in a 20 mL of a chloroform/propionic acid mixture (3 : 1). This was followed by the addition of 1.25 mmol (306 mg) $Mn(OAc)_2{\cdot}4H_2O$ and the reaction mixture was refluxed for 1 h.[27] The organic layer was separated using a separating funnel, collected in chloroform, and evaporated to dryness in a rotary evaporator. The resulting solid was loaded onto a silica gel column and eluted with 1% ethanol in chloroform to remove any unreacted free base. The pure product, isolated as a greenish-black solid, was dried *in vacuo* over anhydrous calcium chloride, and the yield was calculated [yield: 0.162 g, 83.93% for **Mn1**; 0.170 g, 82.12% for **Mn2**; 0.178 g, 79.82% for **Mn3**, 0.142 g, 67.07% for **Mn4**; 0.197 g, 86.40% for **Mn5**] (Scheme S1, ESI†).

Anal. calcd for $C_{47}H_{37}N_4O_4Mn$ (**Mn1**): C, 72.67; H, 4.80; N, 7.21. Found: C, 72.49; H, 4.88; N, 7.13. Selected IR data (KBr, cm^{-1}): 3442br (O–H), 3052w & 2924w (C–H), 1631w, 1598m (C═C), 1439w (C═C), 1384vs, 1350m (C–N), 1176w, 1072m, 1005vs, 834w, 793s (C–$H_{bending}$), 742s, 697s, 526w. UV-Visible in DMSO, [λ_{max}/nm (ε/M^{-1} cm^{-1})]: 466 (S, 1.47×10^5), 568 (Q, 1.44×10^4), 603 (Q, 1.10×10^4). ESI-MS in MeCN (*m*/*z*): 667.1685 for $[M-(2H_2O + C_3H_5O_2^-)]^+$ (calcd: 667.1694). μ_{eff} = 4.5μ_B at 298 K.

Anal. calcd for $C_{51}H_{45}N_4O_4Mn$ (**Mn2**): C, 73.55; H, 5.45; N, 6.73. Found: C, 73.32; H, 5.38; N, 6.79. Selected IR data (KBr, cm^{-1}): 3438br (O–H), 2930w (C–H), 1631w, 1564m (C═C), 1413w (C═C), 1384m, 1352m (C–N), 1209w, 1180w, 1107w, 1074w, 1001s, 799s (C–$H_{bending}$), 717m, 603w, 524w. UV-Visible in DMSO [λ_{max}/nm (ε/M^{-1} cm^{-1})]: 465 (S, 1.29 × 10^5), 569 (Q, 1.42 × 10^4), 607 (Q, 1.36 × 10^4). ESI-MS in MeCN (*m*/*z*): 723.2330 for [M-(2H_2O + $C_3H_5O_2^-$)]$^+$ (calcd: 723.2320). μ_{eff} = 4.7μ_B at 298 K.

Anal. calcd for $C_{51}H_{45}N_4O_8Mn$ (**Mn3**): C, 68.30; H, 5.06; N, 6.25. Found: C, 68.11; H, 5.12; N, 6.17. Selected IR data (KBr, cm^{-1}): 3444br (O–H), 2924w (C–H), 2832w (C–H of –OCH_3), 1606s (C═C), 1507s, 1460m (C═C), 1384w, 1352s (C═C), 1286m, 1248vs (C–O–C), 1174s, 1105w, 1074w, 1027w, 1001s, 803s (C–$H_{bending}$), 717m, 607m, 540w. UV-Visible in DMSO [λ_{max}/nm (ε/M^{-1} cm^{-1})]: 467 (S, 1.38 × 10^5), 572 (Q, 1.46 × 10^4), 609 (Q, 1.66 × 10^4). ESI-MS in MeCN (*m*/*z*): 787.2111 for [M-(2H_2O + $C_3H_5O_2^-$)]$^+$ (calcd: 787.2117). μ_{eff} = 4.9μ_B at 298 K.

Anal. calcd for $C_{47}H_{33}N_4O_4F_4Mn$ (**Mn4**): C, 66.51; H, 3.92; N, 6.60. Found: C, 66.39; H, 3.84; N, 6.69. Selected IR data (KBr, cm^{-1}): 3442br (O–H), 2975w & 2922w (C–H), 1602m (C═C), 1564s, 1498s (C═C), 1415m, 1341m (C–N), 1296w, 1225s, 1158s (Ar–F), 1072m, 1011s, 854w, 803s (C–$H_{bending}$), 719w, 597m, 532m. UV-Visible in DMSO [λ_{max}/nm (ε/M^{-1} cm^{-1})]: 465 (S, 1.22 × 10^5), 567 (Q, 1.24 × 10^4), 603 (Q, 8.64 × 10^3). ESI-MS in MeCN (*m*/*z*): 739.1324 for [M-(2H_2O + $C_3H_5O_2^-$)]$^+$ (calcd: 739.1318). μ_{eff} = 4.4μ_B at 298 K.

Anal. calcd for $C_{47}H_{33}N_4O_4Cl_4Mn$ (**Mn5**): C, 61.73; H, 3.64; N, 6.13. Found: C, 61.73; H, 3.61; N, 6.21. Selected IR data (KBr phase, cm^{-1}): 3421br (O–H), 2977w & 2938w (C–H), 1715m, 1641w, 1566m (C═C), 1484s (C═C), 1394m, 1339w (C–N), 1282w, 1205m, 1091vs (Ar–Cl), 1009vs, 883w, 850w, 803vs (C–$H_{bending}$), 717m, 632w, 562w, 501m. UV-Visible in DMSO [λ_{max}/nm (ε/M^{-1} cm^{-1})]: 463 (S, 1.51 × 10^5), 567 (Q, 1.68 × 10^4), 605 (Q, 1.34 × 10^4). ESI-MS in MeCN (*m*/*z*): 805.0097 for [M-(2H_2O + $C_3H_5O_2^-$)]$^+$ (calcd: 805.0106). μ_{eff} = 4.6μ_B at 298 K.

X-ray crystallographic procedure

The structures of the Mn(III) porphyrins **Mn1**, **Mn2**, **Mn4** and **Mn5** were determined by single-crystal X-ray diffraction. Diffraction-quality crystals were isolated by slow evaporation of aqueous propionic acid solutions of the metalloporphyrins over 2–3 days. Crystals were mounted on glass fibres using epoxy cement. All geometric and intensity data were collected at room temperature on a Bruker SMART APEX II CCD diffractometer equipped with a Mo-K_α fine-focus sealed-tube X-ray source (λ = 0.71073 Å), using increasing ω (width of 0.3° per frame) at a scan speed of 5 s per frame. Intensity data, collected in ω–2θ scan mode, were corrected for Lorentz-polarisation effects and for absorption using SADABS.[28] Structure solution and refinement were performed using a combination of Patterson and Fourier methods, followed by full-matrix least-squares refinement using Bruker SHELXTL suite.[29] For **Mn5**, data were collected using a dual-source (Cu/Mo) Rigaku Saturn 724+ CCD and a Synergy-S kappa diffractometer at room temperature. All hydrogen atoms belonging to the complex were refined isotropically, whereas all the non-hydrogen atoms were refined anisotropically. Perspective molecular views were generated using ORTEP.[30]

HSA binding experiment

The binding affinity of the compounds **Mn1–Mn5** for human serum albumin (HSA) were determined by tryptophan fluorescence quenching experiments using a solution of HSA (2 μM) in Tris-HCl buffer (pH 7.2). Quenching of the emission intensity of the single tryptophan residue (Trp-214) of HSA at 340 nm (excitation wavelength: 280 nm) by increasing concentrations of **Mn1–Mn5** as quenchers was monitored using a fluorescence spectrophotometer. Plots of I_0/I *vs.* [compound] were constructed, and the data were linearly fitted using the Stern–Volmer-like equation $I_0/I = 1 + K[Q]$, where I_0 and I represent the emission intensities of HSA in the absence and presence of the quencher, respectively, and [Q] denotes the quencher concentration. The resulting slopes provided the binding constant K_{HSA} values.[31]

Partition coefficient of the metalloporphyrins between *n*-octanol and water

The partition coefficients of the Mn(III) porphyrins **Mn1–Mn5** between *n*-octanol and water were determined using a modified shake-flask method reported in the literature.[32] In summary, 5 ml solution of the compound in *n*-octanol-saturated water (OSW) was vortexed with 5 ml of water-saturated *n*-octanol (WSO) in a Falcon tube for ~15–20 min. The biphasic mixture was then centrifuged at ~3000 rpm for ~5 min to separate the layers. The concentrations of **Mn1–Mn5** in each layer were quantified by UV-visible spectroscopy. The partition coefficients of the compounds were determined by repeating the experiment three times at varying concentration of **Mn1–Mn5** and averaging the results using the formula $\log P = \log\{[\textbf{Mn1–Mn5}]_{oct}/[\textbf{Mn1–Mn5}]_{aq}\}$.

UV-visible titration using DPBF to ascertain generation of $^1O_2$

1,3-Diphenylisobenzofuran (DPBF) was used as a chemical probe to detect the generation of any singlet oxygen ($^1O_2$) by the Mn(III) porphyrins (**Mn1–Mn5**) under visible light irradiation. DPBF reacts specifically with $^1O_2$ to form an endoperoxide, and a decrease in the absorbance intensity of DPBF at ~415 nm indicates its conversion.[33] The experiment was conducted in two different solvents, *i.e.* DMF and DMSO. A 50 : 1 molar ratio of DPBF to compound was prepared in the respective solvent, and the absorption maxima of DPBF were monitored before and after irradiation with visible light (irradiation provided by a 12 W LED bulb fitted inside a rectangular box of area 9 cm × 4.5 cm, λ = 400–700 nm) at various time intervals. The absorbance data recorded at different time interval of light exposure were fitted in a pseudo first-order rate equation: $\ln([A]_t/[A]_0) = -kt$, where $[A]_0$ and $[A]_t$ represent the absorbance of DPBF before and after light irradiation for a duration of "*t*", and *k* is the DPBF decay constant, indicating the rate of $^1O_2$ generation. The value of *k* was obtained from the slope of the plot.[34] Various control experiments were also

performed to confirm the formation of $^1O_2$, including (a) photoirradiation of untreated DPBF for similar time intervals, (b) photoirradiation of compound-treated DPBF in the presence of a $^1O_2$ quencher (NaN_3) and (c) compound-treated DPBF kept in dark. Relative quantum yields of the compounds for $^1O_2$ generation were calculated from the k values using TPP as the reference standard (Φ_Δ^R = 0.64 in DMF and 0.52 in DMSO), based on the following equation:[35,36]

$$\Phi_\Delta^S = \Phi_\Delta^R \frac{k^S F^R}{k^R F^S}$$

Here, the superscripts S and R denote sample and reference, respectively, and F is the absorption correction factor given by $1–10^{-OD}$, where OD is the absorbance of the compounds.

Photoreduction study in the presence of L-ascorbic acid

Ability of the Mn(III) porphyrins (**Mn1–Mn5**) to undergo photoreduction in the presence of a reducing agent such as L-ascorbic acid was monitored by UV-visible spectroscopy.[37] A 10 μM solution of each Mn(III) porphyrin was treated with ascorbic acid (1.4 mM in case of **Mn1**, **Mn4** and **Mn5**; 2 mM for **Mn2** and **Mn3**) in 1 : 1 DMSO : Tris-HCl buffer medium. The varying amounts of ascorbic acid required for reduction likely reflect differences in the reduction potentials of the compounds. The resulting solutions were then exposed to visible light (λ = 400–700 nm) for 60 min in air, and UV-visible spectra were recorded at 15 min intervals during photoirradiation. A dark control experiment was also performed to validate the photoreduction behavior.

DCFDA assay for detection of ROS

The DCFDA assay was used to detect the generation of cellular reactive oxygen species (ROS), using the most active Mn(III) porphyrin, *i.e.* **Mn4**, as a representative compound for the series. The experiment was conducted *via* flow cytometry following a reported protocol.[38] Approximately 1×10^6 HeLa cells were incubated with **Mn4** (10 μM) for 24 h. The cells were then treated with 10 μM DCFDA solution (in DMSO) in dark for 5 min at room temperature, followed by photoirradiation (400–700 nm) in PBS for varying durations (15, 30, 45 and 60 min). After irradiation, the cells were incubated for an additional 23 h in fresh medium. Corresponding dark control experiments were also conducted. Cells were harvested by trypsinization and resuspended as a single-cell suspension in PBS. Flow cytometry was used to assess the intracellular accumulation of H_2DCF in HeLa cells *via* the FL-1 channel.

Cell viability assay

The cytotoxicity of the compounds **Mn1–Mn5** under visible light was evaluated in HeLa (human cervical carcinoma) cells using the MTT assay. This assay is based on the intracellular reduction of MTT dye by mitochondrial dehydrogenases in viable cells, resulting in the formation of dark blue, membrane-impermeable formazan crystals. The extent of absorbance at 540 nm provides a quantitative estimate of cell viability.[39] HeLa cells were cultured in DMEM with 10% FBS, 100 IU ml^{-1} penicillin, 100 mg ml^{-1} streptomycin and 2 mM glutamax at 37 °C in a humidified incubator with 5% CO_2. Monolayer adherent cultures were passaged every 4–5 days by trypsinization with 0.25% trypsin–EDTA. For the assay, ~1×10^4 HeLa cells were seeded per well in a 96-well culture plate containing DMEM with 10% fetal bovine serum and incubated overnight. Different concentrations of **Mn1–Mn5** were prepared by serial dilution in 1% DMSO–DMEM medium and added to the cells, followed by a 24 h incubation in the dark. Following incubation, the medium was replaced with 50 mM phosphate-buffered saline (PBS; pH 7.4, containing 150 mM NaCl), and one set of cells was photoirradiated for 1 h with visible light (λ = 400–700 nm) at a dose of 10 J cm^{-2}. PBS was then replaced with 10% DMEM, and incubation was continued for an additional 23 h in the dark for light-exposed cells, and for 24 h in the dark for the unexposed cells. Subsequently, 25 μL of MTT solution (4 mg mL^{-1}) was added to each well and incubated for an additional 3 h. After discarding the culture medium, formazan crystals were dissolved in DMSO, and absorbance was measured at 540 nm using a TECAN microplate reader (BioRad, Hercules, CA, USA). The cytotoxicity of the compounds was expressed in terms of their half-maximal inhibitory concentration (IC_{50}) values, calculated using GraphPad Prism 8 software.

Results and discussion

Synthesis and general aspects

Five Mn(III) *meso*-tetraaryalporphyrins (**Mn1–Mn5**) bearing different substituents at the *para* positions of the *meso*-aryl groups along with two water molecules as axial ligands were synthesized in good yields by reacting manganese(II) acetate tetrahydrate with the corresponding free bases (**L1–L5**) in a chloroform/propionic acid mixture. The formation of the free bases (**L1–L5**) was confirmed by ^{1}H NMR and mass spectral data (Fig. S1–S10, ESI†). The corresponding metalloporphyrins (**Mn1–Mn5**) were characterised using various spectroscopic and analytical techniques, which supported the proposed structures. Selected physicochemical data are presented in Table 1. Characteristic N–H stretching vibrations at ~3310–3325 cm^{-1} were observed in the IR spectra of the free bases (Fig. S11–S15, ESI†), which disappeared in case of their Mn(III) derivatives (Fig. S16–S20, ESI†). The absorption spectra of free-base porphyrins (**L1–L5**) in DMSO displayed a typical Soret (or B) band at ~414–421 nm and four Q-bands spanning ~511–651 nm. On metallation with manganese, the electronic spectra exhibited dramatic changes resembling those of hyperporphyrins.[40] The Soret band was significantly red shifted (~50 nm) to ~460 nm, and the two Q-bands extended well into the red region, up to ~605–610 nm (Fig. 1 and Fig. S21, ESI†). More specifically, the absorption intensities of the Q-bands in this region were markedly enhanced compared to their free-base counterparts, a feature highly desirable for PDT.[9,14] These metalloporphyrins also exhibited additional absorption bands in the ~370–400 nm range, which were attrib-

Table 1 Selected physicochemical data for the Mn(III) porphyrins **Mn1–Mn5**

Compound	λ_{abs} [a]/nm ($\varepsilon/10^3$ M^{-1} cm^{-1})	E_f/V (ΔE_p/mV) [b] Mn(III)–Mn(II)	μ_{eff} [c]/μ_B	log $P_{o/w}$	Φ_Δ [d,e]
Mn1	466 (B, 147), 568 (Q_y 14), 603 (Q_x 11)	−0.373 (110)	4.5	0.38	0.09, 0.04
Mn2	465 (B, 129), 569 (Q_y 14), 607 (Q_x 13)	−0.400 (198)	4.7	1.45	0.11, 0.06
Mn3	467 (B, 138), 572 (Q_y 14), 609 (Q_x 16)	−0.402 (157)	4.9	0.36	0.13, 0.08
Mn4	465 (B, 122), 567 (Q_y 12), 603 (Q_x 8.6)	−0.351 (161)	4.6	0.88	0.17, 0.09
Mn5	463 (B, 151), 567 (Q_y 16), 605 (Q_x 13)	−0.336 (173)	4.4	1.71	0.14, 0.08

[a] 5 μM solution in DMSO. [b] Mn(III)–Mn(II) couple in DMF with 0.1 M TBAP, $E_f = 0.5(E_{pa} + E_{pc})$, $\Delta E_p = (E_{pa} - E_{pc})$, where E_{pa} and E_{pc} are the anodic and cathodic peak potentials, respectively. The potentials are referenced against the Ag/AgCl electrode. Scan rate = 100 mV s^{-1}. [c] Magnetic moment measured at 298 K. [d] In DMF. [e] In DMSO.

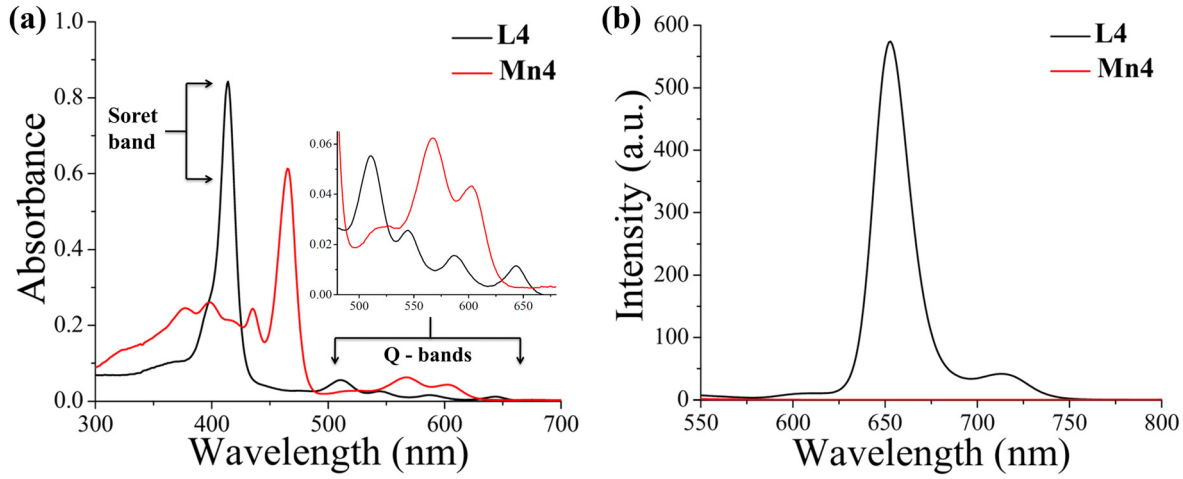

Fig. 1 (a) UV-visible absorption spectra of **L4** and **Mn4** (5 μM) (inset: enlarged view of the Q-bands) and (b) emission spectra of **L4** and **Mn4** (5 μM) in DMSO with λ_{ex} set at their Soret band maxima.

uted to LMCT transitions.[40] Unlike the free-base porphyrins, the Mn(III) derivatives were found to be non-emissive in nature, as revealed by their emission spectra (Fig. 1 and Fig. S22, ESI†). The presence of a high-spin $3d^4$-Mn(III) center with four unpaired electrons was confirmed by the observed magnetic moment values of ~4.5μ_B at 25 °C. The solution-phase stability of compounds **Mn1–Mn5** was evidenced by their high-resolution ESI-MS spectra, which showed the base peak as $[M\text{-}(2H_2O + C_3H_5O_2^-)]^+$, corresponding to the loss of two weakly bound axial water molecules and a propionate counterion in acetonitrile (Fig. S23–S27, ESI†). Cyclic voltammetric measurements displayed a Mn(III)/Mn(II) redox couple at ~−0.3 to −0.4 V *vs.* Ag/AgCl electrode, using TBAP (0.1 M) as the supporting electrolyte. All compounds exhibited quasi-reversible behavior with ΔE_p > 60 mV for the Mn(III)/Mn(II) redox couple (Fig. 2 and Fig. S28, ESI†). The observed large ΔE_p value is most likely associated with a change in the coordination number of the manganese center from six to five upon reduction of the Mn(III) porphyrins from d^4 to d^5.[41] The negative potential required for one-electron reduction of Mn(III) porphyrins is consistent with the electrochemical stabilization of the reduced species. **Mn4** and **Mn5** were comparatively more readily reduced, likely due to the electron-withdrawing nature of the F and Cl atoms, respectively.

Solubility, stability and aggregation properties

The Mn(III) porphyrins **Mn1–Mn5** exhibited good solubility in MeOH, EtOH, MeCN, CH_2Cl_2, $CHCl_3$, THF, DMF and DMSO, but were insoluble in hydrocarbon solvents. The compounds were found to be quite stable in DMSO–DMEM (1 : 1, v/v) solution phase for up to 24 h, as evidenced by their electronic absorption spectra in the ~300–700 nm range (Fig. S29, ESI†). Photostability of the compounds was also evaluated in the same medium by irradiating the solutions with visible light for 60 min. The compounds remained stable under photoirradiation, suggesting their suitability for PDT without any significant degradation into undesirable oxidative products (Fig. S30, ESI†).[42] Moreover, the Mn(III) porphyrins are expected to exhibit reduced aggregation in biological media due to the presence of two axial aqua ligands, which prevent individual porphyrin units from approaching each other closely.[43] In the support of this, **Mn1–Mn5** displayed sharp and intense absorption bands in DMSO–DMEM (1 : 1, v/v) media compared to the broad and less intense bands observed for the free-base porphyrins at similar concentrations, indicating significantly lower aggregation properties for the Mn(III) porphyrins (Fig. S31, ESI†). This finding suggests that Mn(III) porphyrins possess superior aqueous solubility compared to their free-base

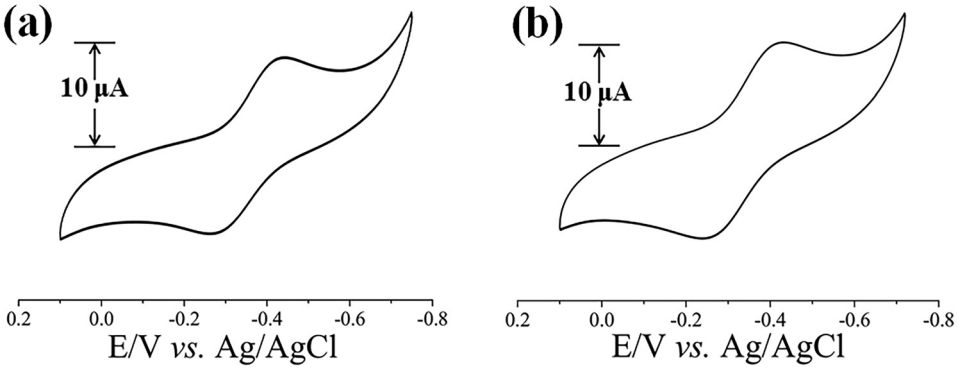

Fig. 2 Cyclic voltammetric responses of **Mn4** (a) and **Mn5** (b) in DMF using 0.1 M TBAP as the supporting electrolyte at a scan rate of 100 mV s^{-1} *vs.* Ag/AgCl.

counterparts, thereby facilitating their evaluation for *in vitro* anticancer activities.

Crystal structure

Structural characterization of the Mn(III) porphyrins **Mn1**, **Mn2**, **Mn4** and **Mn5** was successfully achieved by single-crystal X-ray diffraction analyses in the form of six coordinated cationic species $[Mn(III)Por(H_2O)_2]^+C_3H_5O_2^-$. The crystal structure of **Mn4** is entirely new, whereas those of other Mn(III) porphyrins, *i.e.* **Mn1**, **Mn2** and **Mn5**, have been previously reported, albeit with different counterions crystallized from different solvents.[44–49] To the best of our knowledge, the crystal structure of an Mn(III) porphyrin with propionate as the counterion has not been reported before. The ORTEP views of **Mn4**, **Mn5** and the remaining compounds are shown in Fig. 3 (Fig. S32 and S33, ESI†). **Mn4** crystallizes in the $P\bar{1}$ space group of the triclinic crystal system with 2 molecules per unit cell (Fig. S34, ESI†). **Mn1** also crystallizes in the $P\bar{1}$ space group (triclinic) but with 1 molecule per unit cell (Fig. S35, ESI†). **Mn2** and **Mn5** crystallize in the $P2_1/c$ space group of the monoclinic crystal system, with 2 molecules per unit cell (Fig. S36 and S37, ESI†). Selected crystallographic data are summarized in Table 2 (Table S1, ESI†). Selected bond distances and angle data are provided in Tables S2–S5 (ESI†). All the Mn(III) porphyrins exhibit an octahedral geometry around Mn(III) center, with four coordination sites occupied by the core nitrogen atoms of the flat planar porphyrin ring and two water molecules occupying the fifth and sixth coordination sites, *i.e.* the axial positions, with respect to the plan of the porphyrin ring. The Mn–N bond distances lie in the range of 2.0054–2.0207 Å. The Mn–O bond distances for the coordinated water molecules range from 2.2200–2.314 Å, indicating significant distortion in the octahedral structures imparted by tetragonal elongation anticipated in high-spin d^4 Mn(III) complexes. The Mn–O and Mn–N bond distances are comparable to those reported structures that contain water, methanol, DMF, acrylamide *etc.* as axial ligands along with $[Ag(CN)_2]^-$, Br^-, SbF_6^-, ClO_4^- *etc.* as counterions.[44–49] The plane of the phenyl rings at the *meso* positions is not same with the plane of the porphyrin ring, suggesting a lack of conjugation between the two aromatic systems.

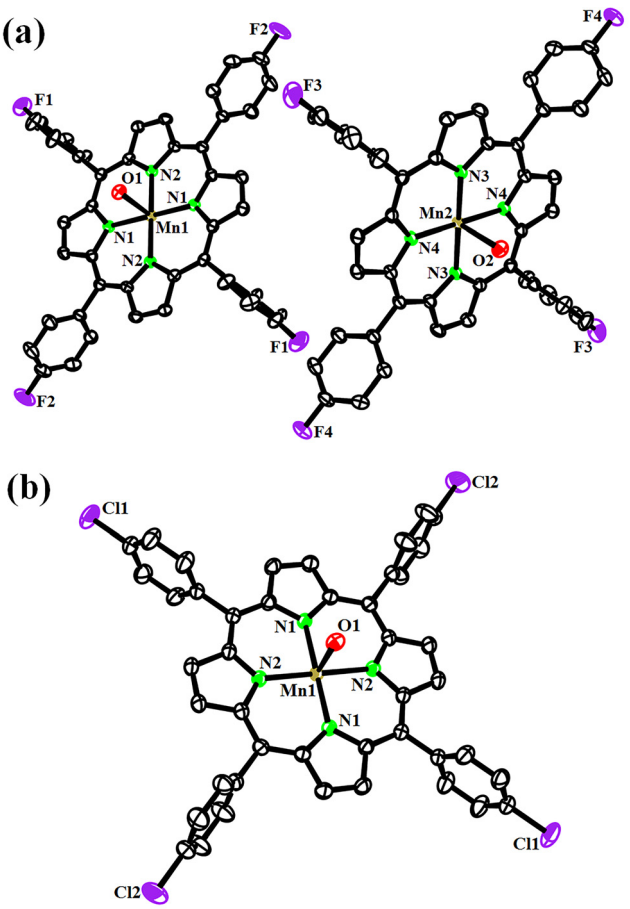

Fig. 3 ORTEP views of (diaqua)*meso*-tetrakis(4-fluorophenylporphyrinato)manganese(III) propionate (**Mn4**) (a) and (diaqua)*meso*-tetrakis(4-chlorophenylporphyrinato)manganese(III) propionate (**Mn5**), (b) showing 30% probability thermal ellipsoids and the atom-numbering scheme for the metal and heteroatoms. The counterion and hydrogen atoms are omitted for clarity.

Binding affinity for HSA

Neutral and anionic porphyrins are known for their ability to form complexes with HSA.[50] The affinity of the synthesized

Table 2 Selected crystallographic data for the compounds (diaqua)*meso*-tetrakis(4-fluoro phenylporphyrinato)manganese(III) propionate (**Mn4**) and (diaqua)*meso*-tetrakis(4-chloro phenylporphyrinato)manganese(III) propionate (**Mn5**)

Empirical formula	$C_{44}H_{28}F_4MnN_4O_2(C_6H_{11}O_4)\cdot3(C_3H_6O_2)$ (**Mn4**)	$C_{44}H_{28}Cl_4MnN_4O_2(C_6H_{11}O_4)\cdot4(C_3H_6O_2)$ (**Mn5**)
F_w, g M^{-1}	1145.02	1284.90
Crystal system	Triclinic	Monoclinic
Space group	$P\bar{1}$	$P2_1/c$
a, Å	9.2702(12)	12.7394(2)
b, Å	14.4396(18)	9.48030(10)
c, Å	22.878(3)	26.7201(4)
α, °	72.099(4)	90
β, °	89.438(5)	98.5660(10)
γ, °	72.965(5)	90
V, Å^3	2775.4(6)	3191.08(8)
Z	2	2
T, K	296(2)	294(2)
ρ_{calcd}, g cm^{-3}	1.370	1.337
λ, Å	0.71073	1.54184
μ, cm^{-1}	0.318	3.768
Data/restraints/parameters	12 091/6/755	6028/1/378
$F(000)$	1192	1336
Goodness-of-fit	1.039	1.076
$R(F_o)^a$, $I > 2\sigma(I)$ [$R_w(F_o)^b$]	0.0707 [0.1664]	0.0536 [0.1531]
R (all data) [R_w (all data)]	0.1261 [0.1932]	0.0594 [0.1582]
Largest diff. peak and hole (e Å^{-3})	0.512, −0.475	0.644, −0.468

^{a} $R = \sum||F_o| - |F_c||/\sum|F_o|$. ^{b} $R_w = \{\sum[w(F_o^2 - F_c^2)^2]/\sum[w(F_o)^2]\}^{\frac{1}{2}}$; $w = [\sigma^2(F_o)^2 + (AP)^2 + BP]^{-1}$, where $P = (F_o^2 + 2F_c^2)/3$, $A = 0.0921$; $B = 0.8341$ (for **Mn4**) and $A = 0.0871$; $B = 1.3753$ (for **Mn5**).

metalloporphyrins **Mn1–Mn5** for human serum albumin (HSA) was evaluated by determining their binding constant values (K_{HSA}) with HSA using a fluorescence quenching experiment. The emission intensity of HSA at 334 nm was gradually quenched, accompanied by a significant blue shift, in Tris-HCl buffer (pH 7.2) on increasing the concentration of **Mn1–Mn5** (Fig. S38, ESI†). The observed decrease in emission intensity and the blue shift are attributed to structural changes in HSA on binding to the Mn(III) porphyrins, leading to perturbations in the microenvironment around the Trp-214 residue responsible for fluorescence. The blue shift in the emission maximum indicates a more hydrophobic environment surrounding the Trp-214 residue upon binding of the Mn(III) porphyrins to HSA.[51,52] A linear plot of I_0/I *vs.* [compound] yielded K_{HSA} values in the following order: **Mn5** > **Mn4** > **Mn2** > **Mn3** ≥ **Mn1** (Table S6, ESI†). Although this order is not completely parallel to their lipophilicity, it can be concluded that an increase in lipophilic character generally favors interaction with HSA. The K_{HSA} values ranged from 9.08 (±0.01) × 10^4 to 4.03 (±0.02) × 10^5 M^{-1}. Compared to these, the manganese derivative of protoporphyrin IX, Mn(III)PPIX, exhibited a relatively higher binding affinity towards HSA, with a K_{HSA} value of 2.13 (±0.07) × 10^6 M^{-1}.[53] The moderate binding affinities of **Mn1–Mn5** for HSA suggest that they can probably bind reversibly to HSA, potentially allowing them to be transported through blood plasma and released at the target tissue.

Measurement of lipophilicity

An essential property for a PDT drug is its ability to incorporate and localize within vital cellular compartments. This is particularly crucial for hydrophobic compounds, for which passive diffusion across the cytoplasmic membrane is often a pre-requisite for cellular uptake.[54] A partition coefficient between *n*-octanol and water serves as an indicator of a drug candidate's potential to diffuse through the lipid bilayer of cell membranes. The *n*-octanol/water partition coefficients (expressed as $\log P_{O/W}$) were determined using the shake-flask method and were found to follow the order: **Mn5** > **Mn2** > **Mn4** > **Mn1** ≥ **Mn3** (Table 1). The Mn(III) porphyrins bearing –Cl and $-CH_3$ substituents at their periphery were found to be highly lipophilic, with $\log P_{O/W} > 1$.

Detection of $^1O_2$ generation using DPBF as a chemical probe

Paramagnetic metalloporphyrins such as those of Co(II) and Cu(II) are reported to be unsuitable candidates for $^1O_2$ generation process.[16,55] To evaluate whether the synthesized Mn(III) porphyrins are capable of generating $^1O_2$ on electronic excitation, both extracellular and intracellular experiments were conducted using UV-visible titration with DPBF and a DCFDA assay as probes (Fig. 4). It is observed that DPBF, in the presence of Mn(III) porphyrins **Mn1–Mn5**, exhibited significant decrease in its absorption maximum under visible light irradiation (Fig. 4a and Fig. S39, ESI†). In contrast, the same experiment performed in the dark showed no significant changes in the DPBF absorption spectrum (Fig. 4a and Fig. S40, ESI†). Control experiments confirmed that DPBF did not undergo self-photodegradation under similar experimental conditions (Fig. S40, ESI†). To further verify whether the observed photodegradation of DPBF in the presence of Mn(III) porphyrins was due to $^1O_2$ generation, a control experiment was performed using NaN_3 as a $^1O_2$ quencher (Fig. 4a and Fig. S41, ESI†). This results of this experiment closely

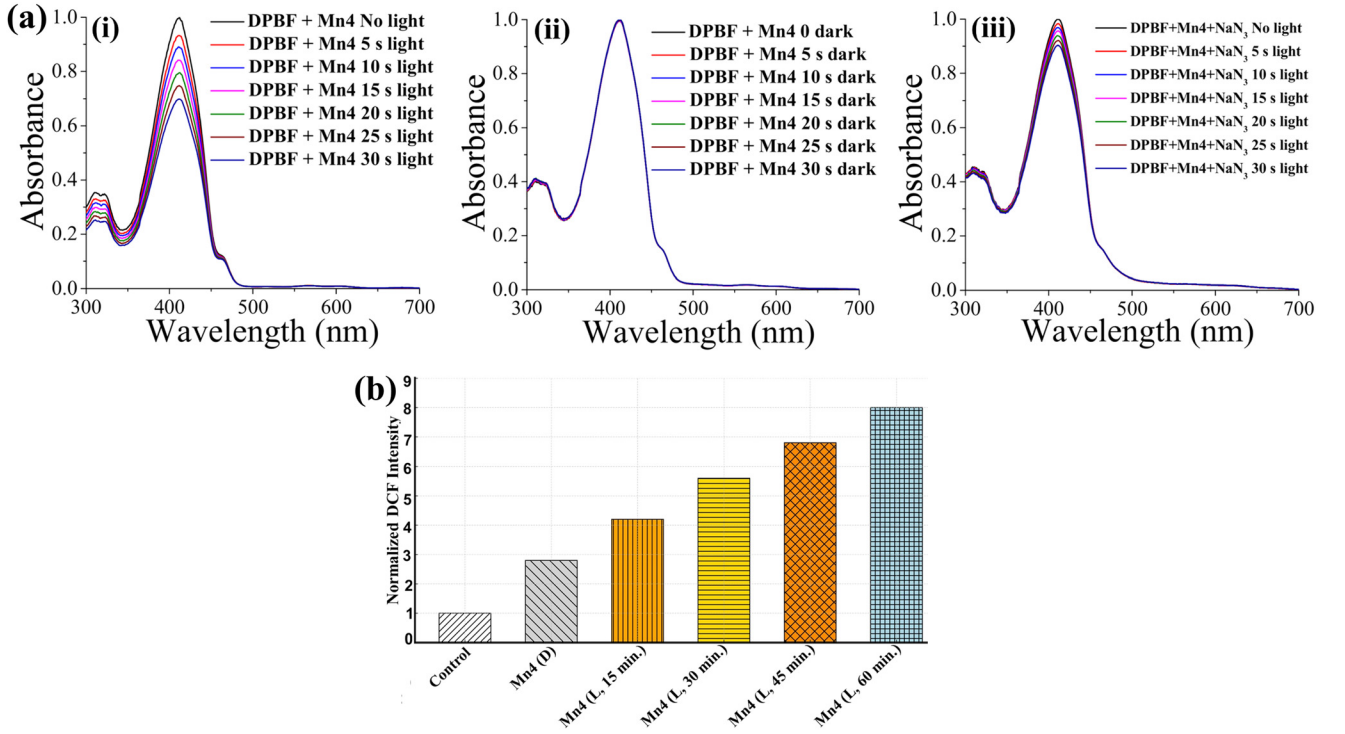

Fig. 4 (a) Absorption spectral traces of DPBF (50 μM) treated with **Mn4** (1 μM) in DMF, monitored at 415 nm: (i) upon photo-irradiation, (ii) kept in the dark and (iii) upon photo-irradiation in the presence of NaN_3 (1 μM). (b) Determination of ROS generation in HeLa cells treated with **Mn4** (10 μM) using the DCFDA assay under various conditions: cells alone; cells with DCFDA and **Mn4** in the dark (D); and cells with DCFDA and **Mn4** exposed to visible light (L) for different time intervals, as represented in the bar diagram.

resembled the photodegradation profile of untreated DPBF. This indicates that the significant decrease in absorption maximum of DPBF in the presence of Mn(III) porphyrins upon photoirradiation under visible light is due to the generation of $^1O_2$. The rate constant values obtained from the linear plot of $-\ln([A]_t/[A]_0)$ *vs. kt* were 5.82×10^{-3} s^{-1}, 8.20×10^{-3} s^{-1}, 8.90×10^{-3} s^{-1}, 1.14×10^{-2} s^{-1} and 9.10×10^{-3} s^{-1} for **Mn1**, **Mn2**, **Mn3**, **Mn4** and **Mn5**, respectively, following the order: **Mn4** > **Mn5** ≥ **Mn3** > **Mn2** > **Mn1** (Fig. S42, ESI†). The $^1O_2$ quantum yields calculated from these rate constants were found to be 0.09, 0.11, 0.13, 0.17 and 0.14 for **Mn1**, **Mn2**, **Mn3**, **Mn4** and **Mn5**, respectively (Table 1). The whole sets of these experiments were further repeated in DMSO, where a similar trend of $^1O_2$ quantum yields was observed (Fig. S43–S46, ESI†). However, $^1O_2$ quantum yield values obtained in DMSO were in the range of 0.04 to 0.09, which were lower compared to those in DMF (Table 1). This difference is likely due to the variable lifetime of $^1O_2$ in different solvents.[56] Although paramagnetic Mn(III) metal centre in porphyrin-type macrocycles promotes non-radiative decay pathways that limit $^1O_2$ generation process, it does not completely eliminate the process. Thus, we observed some residual generation of $^1O_2$ in the Mn(III) porphyrins. The unpaired electrons on Mn(III) in these compounds interact with the ring electrons and hence the (π,π^*) states are not the typical singlets and triplets. The ground state becomes a quintet ($^5S_0$), and the quintet excited states ($^5S_2$ and $^5S_1$) are derived from the excited ring (π,π^*) singlet state, while a "tripmultiplet" manifold ($^3T_1$, $^5T_1$, $^7T_1$) arises from the lowest ring (π,π^*) triplet state. Paramagnetism in Mn(III) porphyrin increases spin–orbit coupling, which in turn significantly enhances the rate of intersystem crossing compared to other metalloporphyrins (*e.g.* for Mn^{III}TPP(Cl) τ_{ISC} = 2.8 ps).[57] Consequently, singlet excited states are rapidly converted to triplet manifolds. Although strong spin–orbit coupling also influences non-radiative decay of excited triplet states, some of these triplet excited states are still relatively long-lived compared to their excited singlet states. A portion of $^5T_1$ state decays back to the ground state, while another portion decays to comparatively long-lived $^7T_1$ state (Fig. S47, ESI†). This state can likely participate in energy transfer with molecular oxygen to generate $^1O_2$. According to Harriman, for Mn^{III}TPP(Cl), the energies of the $^5T_1$ and $^7T_1$ states are 1.8 eV and 1.6 eV, respectively, while the energy required for $^1O_2$ generation is 0.98 eV.[57–60] Although, the Φ_Δ values of the Mn(III) porphyrins are lower than those of typical type-II PDT agents, they may still contribute to their photocytotoxicity due to their relatively better solubility and stability profiles.

Mn(III)/Mn(II) redox shuttle in visible light

Mn(III) porphyrins can reversibly switch between +2 and +3 oxidation states. In general, Mn(III) porphyrins that bearing high positive charges on their periphery, such as water-soluble cat-

ionic Mn(III) porphyrins, are considered good SOD mimics. These compounds exhibit an optimum positive $E_{1/2}$ value for the Mn(III)/Mn(II) redox cycle, making them readily reducible by common reducing agents.[61] However, the $E_{1/2}$ values of the Mn(III)/Mn(II) redox cycle for these Mn(III) porphyrins (**Mn1–Mn5**) fall within the negative range, rendering them difficult to reduce, especially under oxygenated conditions. As a result, reduction of such porphyrins is typically carried out under deaerated conditions.[62] However, when we carried out the reduction experiment of these Mn(III) porphyrins with ascorbic acid, which is a cellular reductant, in 1 : 1 DMSO : Tris-HCl buffer in air with light irradiation, it was observed that with gradual increase in light irradiation, the UV-visible spectra of the porphyrins show some distinct changes that correlate to their reduction to Mn(II) porphyrin. The absorption intensity of the Soret band at ~460 nm gradually decreases and a new band at approximately 434–440 nm appears, which is typical for Mn(II) porphyrins. The other two less intense bands observed at UV region (~370–400 nm) also exhibited decrease in their absorption intensity, and the two Q-bands shifted somewhat towards the red region (Fig. 5 and Fig. S48, ESI†).[37,62] When the light irradiation was stopped and the system was left exposed to air, it exhibited reversibility as shown by their UV-visible spectra (Fig. 5 and Fig. S49, ESI†). These findings suggest that light irradiation can catalyse the reduction of these Mn(III) porphyrins even in aerated conditions. Mn(III) porphyrins are generally stable against photodecomposition, and our photostability data confirmed this behavior (Fig. S30, ESI†). When the same experiment was conducted in the absence of light, the UV-visible spectra of these Mn(III) porphyrins did not show significant changes, suggesting that they are stable against the reduction process even at a higher concentration of ascorbic acid (5 mM), except **Mn5** (Fig. 5 and Fig. S50, ESI†). This photo-redox activity of Mn(III) porphyrins in turn can imbalance the overall redox status of cancer cell. Some literature reports suggest that Mn(II) porphyrins are oxidized to Mn(III) porphyrin by molecular oxygen and, generating H_2O_2 during the process. The hydrogen peroxide produced may then lead to the formation of ROS *via* the Fenton reaction, which can induce oxidative stress that in turn can kill cancer cells.[63,64] However, under our experimental conditions, we were unable to detect H_2O_2, likely due to its very low concentration. No reduction of Mn(III) to Mn(II) porphyrin was observed in the presence of glutathione, either in the dark or under visible light (Fig. S51, ESI†). This is likely due to coordination of the glutathione carboxylate group to the axial position of Mn(III) porphyrin, as previously in the literature.[62] Furthermore, we were also unable to detect any hydroxyl radical formation by the Mn(III) porphyrins at physiological pH, either in the dark or under visible light irradiation, using terephthalic acid as a probe (Fig. S52, ESI†). Nonetheless, literature reports indicate that at alkaline pH (10–11), Mn(III) porphyrins can generate hydroxyl radicals through electron transfer reactions with hydroxide ions.[37]

Intracellular ROS generation

DCFDA assay was employed to evaluate the ability of Mn(III) porphyrins to generate reactive oxygen species in cancer cells, using the most active Mn(III) porphyrin, *i.e.* **Mn4** (10 μM), as a representative compound. H_2DCF, formed intracellularly from DCFDA *via* enzymatic conversion, is oxidized by ROS to yield DCF.[65] The emissive property of DCF in green light (λ_{em} = 528 nm) was used to monitor the ability of **Mn4** to generate ROS in HeLa cells through flow cytometry. A significant increase in DCF emission, resulting from intracellular oxidation of H_2DCF by ROS generated upon photoexcitation of **Mn4**, was observed at various time points, *viz.* 15, 30, 45 and 60 min, in a time-dependent manner, as represented in the bar diagram (Fig. 4b). This was evident from the significant increase in emission count of DCF at different time in the light-exposed HeLa cells treated with **Mn4**. Control experiments using only cells in the dark, cells exposed to light alone and **Mn4**-treated cells kept in the dark did not show any significant ROS generation. The ROS generated by **Mn4** on light exposure is believed to be primarily responsible of the observed cell death.

Photocytotoxicity study

The toxicities of Mn(III) porphyrins **Mn1–Mn5** against HeLa (human cervical carcinoma) cancer cell line under dark and visible light conditions (400–700 nm) were evaluated using the MTT assay, 3-(4,5-dimethylthiazol-2-yl)-2,5-diphenyltetrazolium

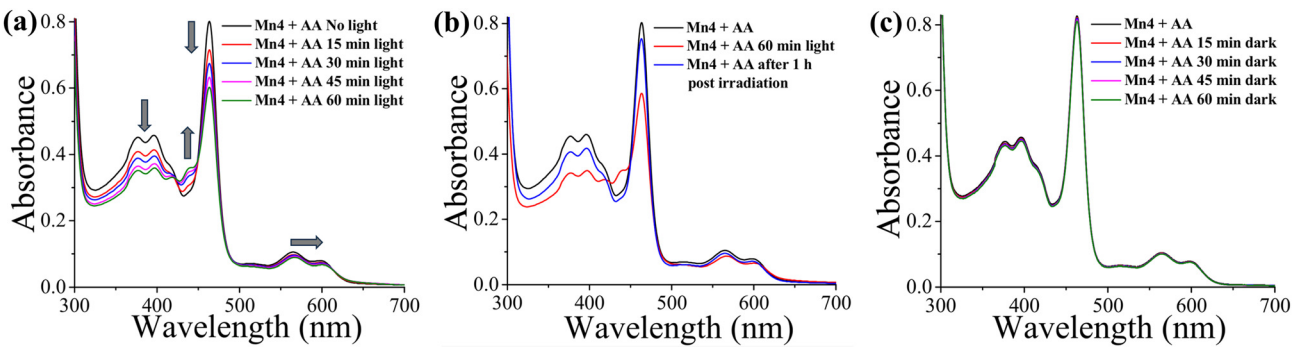

Fig. 5 UV-visible spectra of **Mn4** (10 μM) in 1 : 1 DMSO : Tris-HCl buffer in the presence of ascorbic acid (AA): (a) under light irradiation (1.4 mM AA), (b) post-irradiation reversibility and (c) in the dark (5 mM AA).

bromide (Fig. 6). The compounds **Mn1–Mn5** exhibited remarkable dose-dependent photocytotoxicity in visible light (400–700 nm) in HeLa cell, while showing minimal toxicity in the dark at concentrations up to 50 μM. As the solubility of the compounds were not very high in the permissible composition of DMSO–DMEM mixture, the maximum concentration of the compounds employed was restricted to 50 μM. A >5–10-fold increase in cytotoxicity was observed for **Mn1–Mn5** in HeLa cells following 1 h of light exposure, compared to compound-treated cells kept in the dark under similar experimental conditions. Among the tested compounds, metalloporphyrin **Mn4** was found to be the most phototoxic to HeLa cells, with an IC_{50} value of ~4.9 μM under visible light, while remaining non-toxic in the dark up to a concentration of 50 μM. The phototoxicity index (PI), defined as the ratio of the IC_{50} value in the dark to that in the light, was >10 for **Mn4**. **Mn5**, which contains a chloro substituent in the *para* position of the *meso*-phenyl rings, exhibited significant photocytotoxicity, with an IC_{50} value of ~5.5 μM in visible light and no apparent toxicity in the dark. This implies that the toxicity of the compound is enhanced by more than 9-fold (PI) under visible light. Mn(III) porphyrins bearing $-CH_3$ and $-OCH_3$ substituents in the *para* positions of the *meso*-phenyl rings of the porphyrins, *i.e.* **Mn2** and **Mn3**, exhibited slightly higher IC_{50} values of ~6.25 μM and ~6.70 μM, respectively, under light exposure. Both compounds showed no significant toxicity toward HeLa cells in the dark at concentrations up to 50 μM. The PI values were found to be greater than 8.0 and 7.5 for **Mn2** and **Mn3**, respectively. (Diaqua)*meso*(-tetraphenylporphyrinato)manganese(III) propionate, *i.e.* **Mn1**, showed the lowest phototoxicity among the series, with an IC_{50} value of ~9.54 μM in visible light. It is reported that porphyrins containing paramagnetic metal ions in the core such as Co(II), Cu(II), Mn(III) generally exhibit very poor singlet oxygen quantum yields and are therefore considered unsuitable for PDT.[14,15] However, some studies have demonstrated that Mn(III) porphyrins can exert PDT effects *via* the generation of reactive oxygen species.[22,23,66] Mn(III) porphyrin containing carboxyl groups at the *meso* positions showed a significant enhancement in cyto-

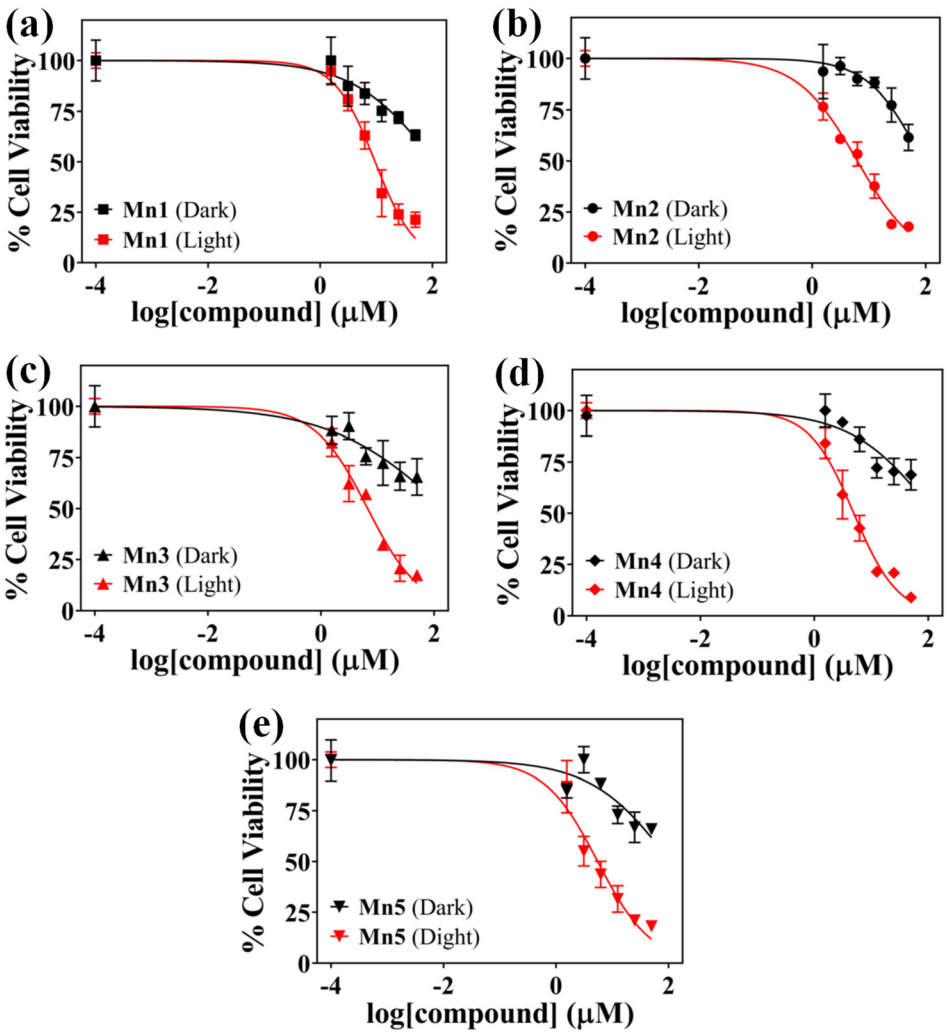

Fig. 6 Cell viability plots showing the cytotoxic effects of **Mn1–Mn5** (a–e) on HeLa cells in the dark (black) and under visible light (400–700 nm, 10 J cm^{-2}, 1 h) (red).

toxicity in HepG2 cells, with an IC_{50} value of ~19.0 μM when irradiated with 625 nm LED light for 60 min. Photoinduced production of superoxide and hydroxide radicals was reported to be responsible for the photocytotoxicity, as revealed by EPR studies.[22] A Mn(III) porphyrin, *viz.* Pt-MnPor-PPh_3, bearing triphenylphosphonium cation and Pt(II) moieties at its *meso*-peripheral positions, exhibited significant PDT effect against HeLa cells upon light irradiation for 10 min using yellow light (4 J cm^{-2}) generated from a 400 W tungsten lamp. The IC_{50} value was reported to be 30.74 μM under light irradiation, whereas no significant cytotoxicity was observed in the dark up to a concentration of 50 μM.[66] Recently, a water-soluble Mn(III) porphyrin bearing cationic pyridyl side groups has been reported to show significant photocytotoxicity in HeLa cells when irradiated with a green LED of 527 nm.[23] The IC_{50} values were found to be 178 and 4 μM in the dark and under light irradiation, respectively, giving a PI value of 44.5. The IC_{50} values of the Mn(III) porphyrins tested, including the Mn(III) porphyrin bearing cationic pyridyl groups, Photofrin®, protoporphyrin IX (PpIX) and cisplatin, are listed in Table 3.[23,67–69] The observed photocytotoxicity is comparable to that of the clinically used PDT drug Photofrin®.[67] PpIX, another established anticancer PDT drug, is found to be slightly more toxic than these metalloporphyrins, with IC_{50} values of 2.8 ± 0.5 μM and 2.1 ± 0.3 μM when irradiated at 510 nm (20 min, 5.0 J cm^{-2}) at 540 nm (40 min, 9.5 J cm^{-2}), respectively.[68] The widely used chemotherapeutic agent cisplatin does not show any significant photocytotoxicity in HeLa cells under similar conditions.[69] Overall, it can be concluded that the Mn(III) porphyrins exhibit significant photodynamic activity in HeLa cells under visible light irradiation through the generation of cytotoxic ROS. The MTT assay for the free-base porphyrins was not performed due to their poor solubility in the acceptable composition of DMSO-DMEM for photochemotherapeutic studies in cancer cells. In general, singlet oxygen quantum yields (Φ_Δ) of free bases (*e.g.* Φ_Δ for TPP 0.64 in DMF) are higher than those of the corresponding Mn(III) porphyrins. However, given their better solubility and lower aggregation properties in aqueous solutions, which normally limit the potential of hydrophobic free-base porphyrins as PS, the use of Mn(III) porphyrins for photodynamic therapeutic application cannot be precluded.[42,70]

Table 3 IC_{50} values of the Mn(III) porphyrins **Mn1–Mn5** and Photofrin® in HeLa cells

	HeLa		
Compound	IC_{50} (μM) dark[a]	IC_{50} (μM) light[b]	PI[c]
Mn1	>50	9.54 ± 1.2	>5.2
Mn2	>50	6.25 ± 1.1	>8.0
Mn3	>50	6.70 ± 0.9	>7.5
Mn4	>50	4.93 ± 0.7	>10.1
Mn5	>50	5.50 ± 0.7	>9.1
$MnT(HeOH)PyP^{5+}$	178[d]	4[d]	44.5[d]
Photofrin®	>41[e]	4.3 ± 0.2[e]	—
PpIX	>100[f,g]	2.8 ± 0.5[f,g]	>35.7[f,g]
	>100[f,h]	2.1 ± 0.3[f,h]	>47.6[f,h]
Cisplatin	71.3 ± 2.9[i]	68.7 ± 3.4[i]	—

[a] The IC_{50} values correspond to 24 h treatment followed by 24 h incubation in the dark. [b] The IC_{50} values correspond to 24 h treatment in the dark followed by photo-exposure to visible light (400–700 nm, 10 J cm^{-2}) for 1 h. Subsequently, cells were incubated for 23 h in the dark. [c] PI (phototoxic index) is the ratio of the IC_{50} in the dark to that under visible light exposure. [d] The IC_{50} values are taken from ref. 23 and correspond to incubation of cells with the compound for 24 h in the dark, followed by illumination with a green LED (527 nm) for 15 min at a power of 45 mW. [e] The Photofrin® IC_{50} values are taken from ref. 67. Light source reported: red light at 633 nm. [f] The IC_{50} values are taken from ref. 68. [g] It corresponds to irradiation at 510 nm (20 min, 5.0 J cm^{-2}). [h] It corresponds to irradiation at 540 nm (40 min, 9.5 J cm^{-2}). [i] The IC_{50} value for 4 h treatment is taken from ref. 69.

Conclusion

In summary, five *meso*-tetraaryl Mn(III) porphyrins bearing various *para* substituents on the *meso*-phenyl ring were synthesized, comprehensively characterized, and evaluated for their visible light-induced anticancer activity. The Mn(III) porphyrins exhibited strong binding affinity toward human serum albumin. Electrochemical studies *via* cyclic voltammetry provided insights into their redox behaviour, while lipophilicity studies highlighted the influence of substituents on their aqueous solubility and membrane permeability. Upon visible light irradiation, these complexes induced significant cytotoxicity in HeLa cells through the generation of ROS, as confirmed by DCFDA assay, while remaining essentially non-toxic in the dark. Photocytotoxicity data demonstrated that fluorine- and chlorine-substituted Mn(III) porphyrins, *i.e.*, **Mn4** and **Mn5**, respectively, displayed enhanced photocytotoxicity toward HeLa cells compared to the other compounds. In addition, these findings highlight the importance of substituent effects on the photophysical and biological properties of Mn(III) porphyrins, offering valuable insights for the rational design of next-generation photosensitizers for targeted cancer therapy. This study opens up the unexplored area of 3d metalloporphyrins for photodynamic therapy.

Conflicts of interest

There are no conflicts to declare.

Data availability

All relevant data supporting the findings of this study are included within the article and its ESI.†

Acknowledgements

The authors are grateful to Department of Science and Technology (DST)-SERB, Government of India, Core Research Grant (CRG) (CRG/2023/002246) for financial assistance. We also acknowledge financial support from the DST-PURSE 2022 program (TPN-84912). The authors are thankful to DST and

Department of SAIF, Gauhati University, for single crystal X-ray diffractometer facility. We also thank Dr Ranjit Thakuria, Dr Tejender S. Thakur, Dr S. Brahma and Dr Debajit Sarma for their kind assistance in X-ray data collection and structure solution. We sincerely thank Prof. A. R. Chakravarty, Indian Institute of Science, Bangalore, for allowing us to use the cell culture facility in his laboratory. JPS thanks DST-SERB for research fellowship.

References

1 M. O. Senge, N. N. Sergeeva and K. J. Hale, *Chem. Soc. Rev.*, 2021, **50**, 4730–4789.
2 C. J. Kingsbury and M. O. Senge, *Coord. Chem. Rev.*, 2021, **431**, 213760.
3 M. A. Rajora, J. W. H. Lou and G. Zheng, *Chem. Soc. Rev.*, 2017, **46**, 6433–6469.
4 S. Ishihara, J. Labuta, W. V. Rossom, D. Ishikawa, K. Minami, J. P. Hill and K. Ariga, *Phys. Chem. Chem. Phys.*, 2014, **16**, 9713–9746.
5 A. F. dos Santos, D. R. Q. de Almeida, L. F. Terra, M. S. Baptista and L. Labriola, *J. Cancer Metastasis Treat.*, 2019, **5**, 25.
6 X. Wang, J. Peng, C. Meng and F. Feng, *Chem. Sci.*, 2024, **15**, 12234–12257.
7 H. Abrahamse and M. R. Hamblin, *Biochem. J.*, 2016, **473**, 347–364.
8 L. M. Moreira, F. V. D. Santos, J. P. Lyon, M. Maftoum-Costa, C. Pacheco-Soares and N. S. D. Silva, *Aust. J. Chem.*, 2008, **61**, 741–754.
9 M. Ethirajan, Y. Chen, P. Joshi and R. K. Pandey, *Chem. Soc. Rev.*, 2011, **40**, 340–362.
10 H. Shi, C. Imberti and P. J. Sadler, *Inorg. Chem. Front.*, 2019, **6**, 1623–1638.
11 M. R. Detty, S. L. Gibson and S. J. Wagner, *J. Med. Chem.*, 2004, **47**, 3897–3915.
12 J. Kou, D. Dou and L. Yang, *Oncotarget*, 2017, **8**, 81591–81603.
13 Q. Zhang, J. He, W. Yu, Y. Li, Z. Liu, B. Zhou and Y. Liu, *RSC Med. Chem.*, 2020, **11**, 427–437.
14 A. P. Castano, T. N. Demidova and M. R. Hamblin, *Photodiagn. Photodyn. Ther.*, 2004, **1**, 279–293.
15 T. L. C. Figueiredo, R. A. W. Johnstone, A. M. P. S. Sørensen, D. Burget and P. Jacques, *Photochem. Photobiol.*, 1999, **69**, 517–528.
16 P. M. Antoni, A. Naik, I. Albert, R. Rubbiani, S. Gupta, P. Ruiz-Sanchez, P. Munikorn, J. M. Mateos, V. Luginbuehl, P. Thamyongkit, U. Ziegler, G. Gasser, G. Jeschke and B. Spingler, *Chem. – Eur. J.*, 2014, **20**, 1–6.
17 L. Li and X. Yang, *Oxid. Med. Cell. Longevity*, 2018, **2018**, DOI: 10.1155/2018/7580707.
18 B. Hasan, A. Tovmasyan, I. Batinic-Haberle and L. Benov, *Redox Rep.*, 2021, **26**, 85–93.
19 A. Tovmasyan, H. Sheng, T. Weitner, A. Arulpragasam, M. Lu, D. S. Warner, Z. Vujaskovic, I. Spasojevic and I. Batinic-Haberle, *Med. Princ. Pract.*, 2013, **22**, 103–130.
20 A. Tovmasyan, R. S. Sampaio, M.-K. Boss, J. C. Bueno-Janice, B. H. Bader, M. Thomas, J. S. Reboucas, M. Orr, J. D. Chandler, Y.-M. Go, D. P. Jones, T. N. Venkatraman, S. Haberle, N. Kyui, C. D. Lascola, M. W. Dewhirst, I. Spasojevic, L. Benov and I. Batinic-Haberle, *Free Radical Biol. Med.*, 2015, **89**, 1231–1247.
21 S. Banfi, E. Cassani, E. Caruso and M. Cazzaro, *Bioorg. Med. Chem.*, 2003, **11**, 3595–3605.
22 L. Shi, Y.-Y. Jiang, T. Jiang, W. Yin, J.-P. Yang, M.-L. Cao, Y.-Q. Fang and H.-Y. Liu, *Molecules*, 2017, **22**, 1084.
23 T. Nemeth, A. Pallier, C. Çelik, Z. Garda, N. Yoshizawa-Sugata, H. Masai, É. Tóth and Y. Yamakoshi, *Chem. Biomed. Imaging*, 2025, **3**, 5–14.
24 Y. H. Kim, S. D. Jung, M. H. Lee, C. Im, Y.-H. Kim, Y. J. Jang, S. K. Kim and D. W. Cho, *J. Phys. Chem. B*, 2013, **117**, 9585–9590.
25 O. Kahn, *Molecular Magnetism*, VCH, Weinheim, 1993.
26 A. D. Adler, F. R. Longo, J. D. Finarelli, J. Goldmacher, J. Assour and L. Korsakoff, *J. Org. Chem.*, 1967, **32**, 476.
27 A. D. Adler, F. R. Longo, F. Kampas and J. Kim, *J. Inorg. Nucl. Chem.*, 1970, **32**, 2445–2448.
28 N. Walker and D. Stuart, *Acta Crystallogr., Sect. A: Found. Crystallogr.*, 1983, **39**, 158–166.
29 G. M. Sheldrick, *Acta Crystallogr., Sect. A: Found. Crystallogr.*, 2008, **64**, 112–122.
30 L. J. Farrugia, *J. Appl. Crystallogr.*, 1997, **30**, 565–565.
31 J. Seetharamappa and B. P. Kamat, *Chem. Pharm. Bull.*, 2004, **52**, 1053–1057.
32 J. Wu, D. G. J. Goodwin, K. Peter, D. Benoit, W. Li, D. H. Fairbrother and J. D. Fortner, *Environ. Sci. Technol. Lett.*, 2014, **1**, 490–494.
33 M. K. Raza, S. Gautam, A. Garai, K. Mitra, P. Kondaiah and A. R. Chakravarty, *Inorg. Chem.*, 2017, **56**, 11019–11029.
34 L.-X. Wang, J.-W. Li, J.-Y. Huang, J.-H. Li, L.-J. Zhang, D. Æshea and Z.-L. Chen, *Tumor Biol.*, 2015, **36**, 6839–6847.
35 S. Meng, Z. Xu, G. Hong, L. Zhao, Z. Zhao, J. Guo, H. Ji and T. Liu, *Eur. J. Med. Chem.*, 2015, **92**, 35–48.
36 P. Sen, R. Soy, S. Mgidlana, J. Mack and T. Nyokong, *Dyes Pigm.*, 2022, **203**, 110313.
37 A. Harriman and G. Porter, *J. Chem. Soc., Faraday Trans. 2*, 1979, **75**, 1543–1552.
38 H. Wang and J. A. Joseph, *Free Radical Biol. Med.*, 1999, **27**, 612–616.
39 T. Mosmann, *J. Immunol. Methods*, 1983, **65**, 55–63.
40 C. C. Wamser and A. Ghosh, *JACS Au*, 2022, **2**, 1543–1560.
41 L. E. Lieske, S. L. Hooe, A. W. Nichols and C. W. Machan, *Dalton Trans.*, 2019, **48**, 8633–8641.
42 N. Mariño-Ocampo, L. Dibona-Villanueva, E. Escobar-Álvarez, D. Guerra-Díaz, D. Zúñiga-Núñez, D. Fuentealba and J. Robinson-Duggon, *Photochem. Photobiol.*, 2023, **99**, 469–497.
43 B. Babu, E. Amuhaya, D. Oluwole, E. Prinsloo, J. Mack and T. Nyokong, *Med. Chem. Commun.*, 2019, **10**, 41–48.

44 C. L. Hill and M. M. Williamson, *Inorg. Chem.*, 1985, **24**, 2836–2841.
45 M. M. Williamson and C. L. Hill, *Inorg. Chem.*, 1987, **26**, 4155–4160.
46 N. Xu, A. W. Bevak, B. R. Armstrong and D. R. Powell, *Polyhedron*, 2017, **127**, 432–437.
47 R. Soman, S. Sujatha and C. Arunkumar, *J. Porphyrins Phthalocyanines*, 2016, **20**, 833–842.
48 X. Chen, Z. D. Zhao, P. Wang and D. P. Zhang, *Russ. J. Coord. Chem.*, 2014, **40**, 320–324.
49 Z. N. Zahran, J. Lee, S. S. Alguindigue, M. A. Khan and G. B. Richter-Addo, *Dalton Trans.*, 2004, **1**, 44–50.
50 O. A. Chaves, T. V. Acunha, B. A. Iglesias, C. S. H. Jesus and C. Serpa, *J. Mol. Liq.*, 2020, **301**, 112466.
51 I. Ling, M. Taha, N. A. Al-Sharji and O. K. Abou-Zied, *Spectrochim. Acta, Part A*, 2018, **194**, 36–44.
52 A. Costa-Tuna, O. A. Chaves, R. J. S. Loureiro, S. Pinto, J. Pina and C. Serpa, *Int. J. Biol. Macromol.*, 2024, **255**, 128210.
53 J. Hu, E. H. Soraiz, C. N. Johnson, B. Demeler and L. Brancaleon, *Int. J. Biol. Macromol.*, 2019, **134**, 445–457.
54 J. A. Arnott and S. L. Planey, *Expert Opin. Drug Discovery*, 2012, **7**, 863–875.
55 S. Mathai, T. A. Smith and K. P. Ghiggino, *Photochem. Photobiol. Sci.*, 2007, **6**, 995–1002.
56 T. Entradasa, S. Waldrona and M. Volk, *J. Photochem. Photobiol., B*, 2020, **204**, 111787.
57 L.-L. Wang, S.-H. Peng, H. Wang, L.-N. Ji and H.-Y. Liu, *Phys. Chem. Chem. Phys.*, 2018, **20**, 20141–20148.
58 X. Yan, C. Kirmaier and D. Holten, *Inorg. Chem.*, 1986, **25**, 4774–4777.
59 G. Porter and M. R. Wright, *Discuss. Faraday Soc.*, 1959, **27**, 18–27.
60 S. Joseph and S. K. A. Kumar, *Coord. Chem. Rev.*, 2023, **496**, 215408.
61 A. Tovmasyan, S. Carballal, R. Ghazaryan, L. Melikyan, T. Weitner, C. G. C. Maia, J. S. Reboucas, R. Radi, I. Spasojevic, L. Benov and I. Batinic-Haberle, *Inorg. Chem.*, 2014, **53**, 11467–11483.
62 S. M. A. Pinto, A. R. R. Ferreira, D. S. S. Teixeira, S. C. C. Nunes, A. L. M. B. de Carvalho, J. M. S. Almeida, Z. Garda, A. Pallier, A. A. C. C. Pais, C. M. A. Brett, É. Tóth, M. P. M. Marques, M. M. Pereira and C. F. G. C. Geraldes, *Chem. – Eur. J.*, 2023, **29**, e202301442.
63 I. A. Duncan, A. Harriman and G. Porter, *J. Chem. Soc., Faraday Trans. 2*, 1980, **76**, 1415–1428.
64 I. Batinic-Haberle, A. Tovmasyan, Z. Huang, W. Duan, L. Du, S. Siamakpour-Reihani, Z. Cao, H. Sheng, I. Spasojevic and A. A. Secord, *Oxid. Med. Cell. Longev.*, 2021, **2021**, DOI: **10.1155/2021/6653790**.
65 D. Yu, Y. Zha, Z. Zhong, Y. Ruan, Z. Li, L. Sun and S. Hou, *Sens. Actuators, B*, 2021, **339**, 129878.
66 M. Yang, J. Deng, D. Guo, Q. Sun, Z. Wang, K. Wang and F. Wu, *Dyes Pigm.*, 2019, **166**, 189–195.
67 A. Bhattacharyya, A. Jameei, A. Garai, R. Saha, A. A. Karande and A. R. Chakravarty, *Dalton Trans.*, 2018, **47**, 5019–5030.
68 J. Karges, U. Basu, O. Blacque, H. Chao and G. Gasser, *Angew. Chem., Int. Ed.*, 2019, **58**, 14334–14340.
69 S. Saha, D. Mallick, R. Majumdar, M. Roy, R. R. Dighe, E. D. Jemmis and A. R. Chakravarty, *Inorg. Chem.*, 2011, **50**, 2975–2987.
70 V. A. Oliveira, H. Terenzi, L. B. Menezes, O. A. Chaves and B. A. Iglesias, *J. Photochem. Photobiol., B*, 2020, **211**, 111991.